CI and CO in the center of M 51

Israel, F.P.; Tilanus, R.P.J.; Baas, F.

Citation
Israel, F. P., Tilanus, R. P. J., & Baas, F. (2006). CI and CO in the center of M 51. *Astronomy And Astrophysics*, *445*, 907-913. Retrieved from https://hdl.handle.net/1887/7226

Version:	Not Applicable (or Unknown)
License:	Leiden University Non-exclusive license
Downloaded from:	https://hdl.handle.net/1887/7226

Note: To cite this publication please use the final published version (if applicable).

A&A 445, 907–913 (2006)
DOI: 10.1051/0004-6361:20053096
© ESO 2006

Astronomy & Astrophysics

CI and CO in the center of M 51

F. P. Israel[1], R. P. J. Tilanus[2], and F. Baas[1,2,†]

[1] Sterrewacht Leiden, PO Box 9513, 2300 RA Leiden, The Netherlands
e-mail: israel@strw.leidenuniv.nl
[2] Joint Astronomy Centre, 660 N. A'ohoku Pl., Hilo, Hawaii, 96720, USA

Received 20 March 2005 / Accepted 13 September 2005

ABSTRACT

We present $J = 2–1$, $J = 3–2$, $J = 4–3$ ^{12}CO maps as well as $J = 2–1$, $J = 3–2$ ^{13}CO and 492 GHz [CI] measurements of the central region in M 51. The distribution of CO is strongly concentrated towards the spiral arms. The center itself is poor in, though not devoid of, CO emission. The observed line intensities require modelling with a multi-component molecular gas. A dense component must be present ($n(\mathrm{H_2}) \approx 10^3$) with kinetic temperature $T_{\rm kin} \approx 100$ K, combined with either a less dense ($\approx 10^2$ cm^{-3}) component of the same temperature, or a more dense ($n(\mathrm{H_2}) \approx 3 \times 10^3$ cm^{-3}) and much cooler ($T_{\rm kin} = 10$–30 K) component. Atomic carbon amounts are between 5 and 10 times those of CO. Much of the molecular gas mass is associated with the hot PDR phase. The center of M 51 has a face-on gas mass density of about $40 \pm 20\ M_\odot$ pc^{-2}, and a well-established CO-to-$\mathrm{H_2}$ conversion ratio X four to five times lower than the standard Galactic value.

Key words. galaxies: individual: M 51 – galaxies: spiral – galaxies: ISM – galaxies: nuclei – submillimeter

1. Introduction

Molecular gas is a major constituent of the interstellar medium in galaxies. This is particularly true for star-forming complexes in the spiral arms, but strong circumnuclear concentrations of molecular gas are frequently found also in the inner kiloparsec of spiral galaxies. We have observed a sample of nearby spiral galaxies in various CO transitions and in the 492 GHz $^3\mathrm{P_1}$–$^3\mathrm{P_0}$ [CI] transition in order to determine the physical condition of molecular gas in their inner parts. Results for NGC 253 (Israel et al. 1995), NGC 7331 (Israel & Baas 1999), NGC 6946, M 83 = NGC 5236 (Israel & Baas 2001) as well as IC 342 and Maffei 2 (Israel & Baas 2003) have been published. In this paper, we present results obtained for the interacting, two-armed spiral M 51 = NGC 5194 (see Table 1).

M 51 was one of the first galaxies mapped in CO line emission, and it has been observed many times since (Rickard et al. 1977; Scoville & Young 1983; Rydbeck et al. 1985; Sandqvist et al. 1989; García-Burillo et al. 1993a,b; Berkhuijsen et al. 1993; Nakai et al. 1994; Young et al. 1995; Mauersberger et al. 1999; Wielebinski et al. 1999; Dumke et al. 2001; Paglione et al. 2002; Tosaki et al. 2002; Kramer et al. 2005), including mapping observations with millimeter arrays (Lo et al. 1987; Rand & Kulkarni 1990; Rand 1993; Scoville et al. 1998; Aalto et al. 1999; Sakamoto et al. 1999; Regan et al. 2001).

2. Observations

All observations described in this paper were carried out with the 15 m James Clerk Maxwell Telescope (JCMT) on Mauna Kea (Hawaii)[1]. At the epoch of the mapping observations (1990–1996) the absolute pointing of the telescope was good to about 3″ rms as provided by pointing observations with the JCMT submillimetre bolometer. The spectra were calibrated in units of antenna temperature $T_{\rm A}^*$, correcting for sideband gains, atmospheric emission in both

Table 1. Galaxy parameters.

	M 51
Type[a]	SA(s)bcp
Radio Center :	
RA (B1950)[b]	$13^{\rm h}27^{\rm m}46.3^{\rm s}$
Decl (B1950)[b]	+47°27′10″
RA (J2000)[b]	$13^{\rm h}29^{\rm m}52.7^{\rm s}$
Decl (J2000)[b]	+47°11′42″
$V_{\rm LSR}^{c,}$	+464 km s^{-1}
Inclination i^c	20°
Position angle P^c	170°
Distance D^d	9.7 Mpc
Scale	21.3″/kpc

Notes: [a] RSA (Sandage & Tammann 1987); [b] Turner & Ho (1994); [c] Tully (1974); [d] Sandage & Tamann (1975).

[1] The James Clerk Maxwell Telescope is operated on a joint basis between the United Kingdom Particle Physics and Astrophysics Council (PPARC), the Netherlands Organisation for Scientific Research (NWO) and the National Research Council of Canada (NRC).

Article published by EDP Sciences and available at http://www.edpsciences.org/aa or http://dx.doi.org/10.1051/0004-6361:20053096

Table 2. Observations Log.

Transition	Date	Freq	T_{sys}	Beam Size	η_{mb}	t(int)	Map parameters		
							Points	Size	Spacing
	(MM/YY)	(GHz)	(K)	(″)		(s)		(″)	(″)
^{12}CO $J = 2-1$	12/90; 05/91	230	920	21	0.69	480	40	30×50	10
^{12}CO $J = 3-2$	12/93	345	1475	14	0.53	400	18	40×50	12
	05/97; 05/01		660		0.60	70	400	60×120	6
^{12}CO $J = 4-3$	03/94; 04/96	461	3950	11	0.50	600	16	24×20	6
	12/01		2100		0.52	1200	6	18×12	6
^{13}CO $J = 2-1$	06-95	220	370	21	0.69	2520	1	–	–
^{13}CO $J = 3-2$	05-97; 05/01	330	600	14	0.63	3600	9	15×15	7.5
CI $^3P_1$–$^3P_0$	11-94	492	6675	10	0.53	960	4	–	–

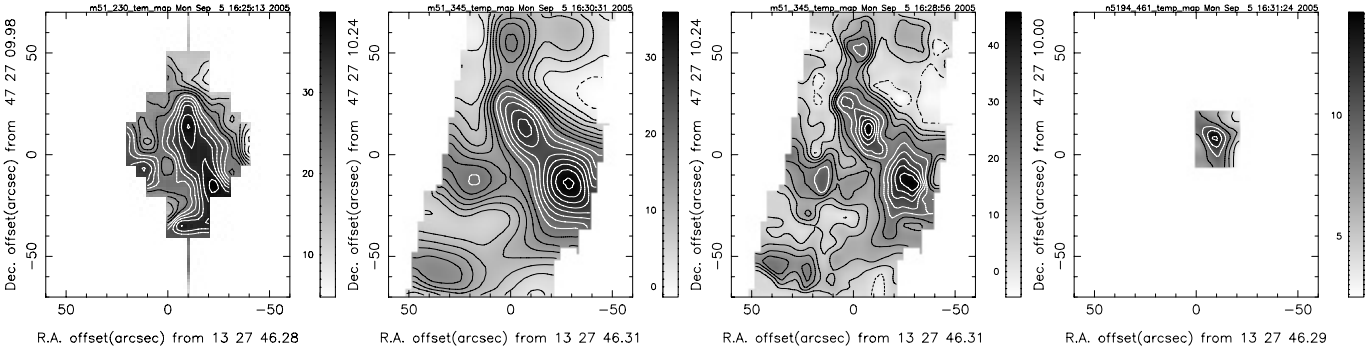

Fig. 1. Contour maps of emission from M 51 integrated over the velocity range V_{LSR} = 300 to 600 km s^{-1}. North is at top. Offsets are marked in arcsec relative to the M 51 nucleus at (0,0) with B1950 coordinates given corresponding to J2000 coordinates $\alpha_\circ = 13^h29^m52\overset{s}{.}7, \delta_\circ = +47°11'43''$ (cf. Table 1). *Left to right*: CO $J = 2-1$ at 21″ (985 pc) resolution, CO $J = 3-2$ convolved to 21″, CO $J = 3-2$ at 14″ (656 pc) resolution and CO $J = 4-3$ convolved to 14″ resolution. Contour values are linear in $\int T_{mb} dV$. Contour steps are 4 K km s^{-1} (2–1 full resolution, 3–2 convolved, 4–3 convolved) and 8 K km s^{-1} (3–2 full resolution) and start at 0.

sidebands and telescope efficiency. Calibration was regularly checked by observation of a standard line source. Further observational details are given in Table 2. Most of the observations were carried out with the now defunct receivers A2, B3i and C2. Observations in 2001 were obtained with the current receivers B3 (330/345 GHz) and W/C (461 GHz). Full details on these receivers can be found at the JCMT website (`http://docs.jach.hawaii.edu/JCMT/HET/GUIDE/`).
Note that the angular beamsizes used correspond to linear resolutions ranging from 470 to 1000 pc at the distance assumed for M 51. Up to 1993, we used a 2048 channel AOS backend covering a band of 500 MHz (650 km s^{-1} at 230 GHz). After that year, the DAS digital autocorrelator system was used in bands of 500 and 750 MHz. Integration times (on+off) given in Table 2 are typical values appropriate to the maps. Because of the relatively good weather conditions and its very close sampling, the 345 GHz $J = 3-2$ ^{12}CO map (shown in Fig. 1) should be considered the most reliable. Both the 230 GHz $J = 2-1$ ^{12}CO and the 461 GHz $J = 4-3$ ^{12}CO maps were obtained under less favourable weather conditions (as evidenced by the system temperatures listed in Table 2). Features in the 230 GHz map show offsets from their counterparts in the 345 GHz map by as much as 8″, and the peak in the 461 GHz map is offset from its 345 GHz counterpart by 5.5″. As these map position differences are less than three resp. two times the rms pointing accuracy, we do not consider them to be physically significant.

M 51 is observed almost face-on, lines are narrow and sufficient free baseline was available to subtracted second or even third order baselines from the profiles. Finally, all spectra were scaled to a main-beam brightness temperature, $T_{mb} = T_A^*/\eta_{mb}$; values for η_{mb} are given in Table 2.

Much of the following analysis is based on line ratios at two specific positions A and B. Position A is that of the (radio) nucleus, position B is centered on a large and bright CO complex (called Giant Molecular Association 1 by Tosaki et al. 1994) in one of the inner spiral arms at a radial distance of 0.9 kpc northwest of the nucleus. Measurements of these positions are much more accurate than those of individual map positions. They were usually observed more than once, with better pointing (typically 1.5″−2″ rms) and with significantly longer integration times resulting not only in higher signal-to-noise ratios but also in better baselines and higher position reliability. Relatively accurate line intensities for full-resolution profiles at the two positions are summarized in Table 3. In this table, we also give extrapolated line intensities at other resolutions, derived as follows. We compared intensities at the two positions in maps at full-resolution and in maps convolved to the

Table 3. Central CO and CI line intensities in M 51.

Transition		Resolution (″)	T_{mb} (mK)	$\int T_{mb}dV$ (K km s^{-1})	T_{mb} (mK)	$\int T_{mb}dV$ (K km s^{-1})
			Position A: Center		Position B: NW Arm GMA-1	
^{12}CO	$J = 2–1$	21	260	38.8 ± 8.5	805	54.0 ± 7.5
		43	–	44.5 ± 9.0	–	36.0 ± 7.2
^{13}CO		21	–	–	77	7.5 ± 1.0
^{12}CO	$J = 3–2$	14	375	42.7 ± 6.5	1535	64.5 ± 9.5
		21	–	30.2 ± 6.0	–	55.0 ± 9.5
^{13}CO		14	28	3.3 ± 0.7	43	5.5 ± 1.5
^{12}CO	$J = 4–3$	11	160	27.0 ± 4.5	520	52.5 ± 7.5
		14	–	23.0 ± 4.5	–	33.0 ± 7.0
		21	–	19.0 ± 3.8	–	24.0 ± 4.0
[CI]	$^3P_1$–$^3P_0$	10	–	–	565	28 ± 5
		21	–	–	–	(13 ± 4)

Note: Position A: beam centered on nucleus; Position B: beam centered on Giant Molecular Association 1 in NW spiral arm at offsets $\Delta\alpha = -10''$, $\Delta\delta = +15''$ with respect to the nucleus.

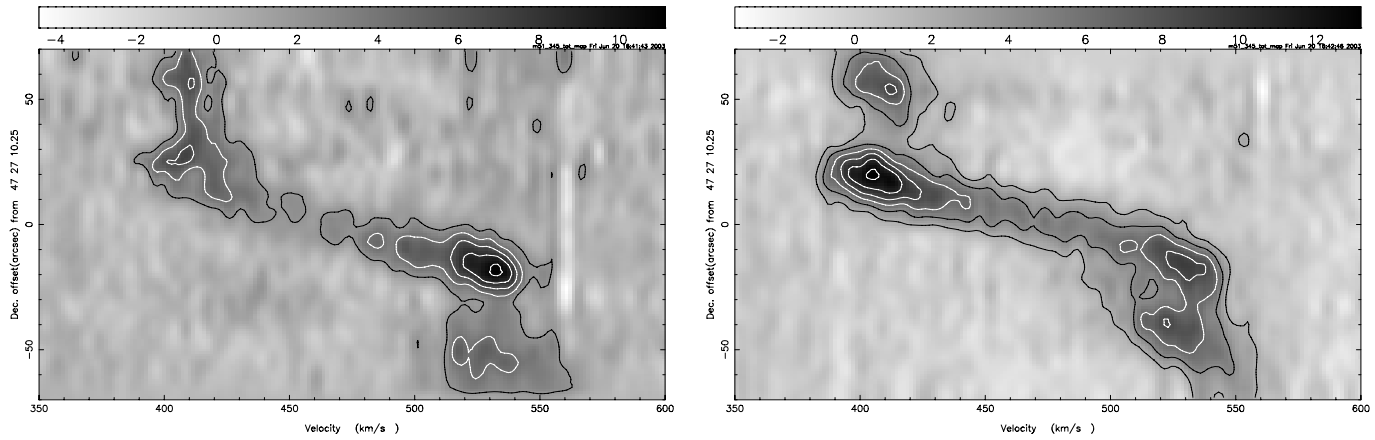

Fig. 2. Position-velocity maps of CO $J = 3–2$ emission from M 51 in position angle 10°. *Left*: east of the nucleus, averaged $\Delta\alpha = 20''$–$0''$; *right*: west of the nucleus, averaged over $\Delta\alpha = 0''$–$20''$. Contour values are linear in steps of $T_{mb} = 4$ K, starting at step 1. Horizontal scale is V_{LSR}

desired resolution. The accurate full-resolution measurements in Table 3 were then multiplied by the empirical scaling factors thus determined. We verified that this is a robust procedure. Pointing errors do result in different intensities at any given position, but scaling factors change much more slowly.

3. Results

3.1. CO distribution

The distribution of molecular gas as traced by CO shows a minimum at the position of the galaxy nucleus (position $0'', 0''$ in Fig. 1). CO is strongly concentrated towards the major spiral arms. The CO maps in Fig. 1 clearly show the outline of the inner parts of the western spiral arm, as well as part of the inner eastern arm. In all observed transitions, the emission peaks coincide with the brightest CO peaks seen in the $J = 1–0$ maps (see e.g. Scoville et al. 1998 or Regan et al. 2001) which are associated with star-forming regions.

The north-south position-velocity maps (Fig. 2), paralleling the major axis of M 51, show emission covering a velocity range of 150 km s^{-1}, which becomes 440 km s^{-1} after correction for inclination. The velocity distributions east and west of the major axis are practically identical, at least at our resolution. Within a radius $R < 30''$ the molecular gas is in rapid solid-body rotation. Again, the relative lack of molecular gas in the center (position +464 km s^{-1}, $0''$) is obvious, as is the strong molecular emission near the radius where differential rotation takes over. As the pV-maps of M 51 are virtually indistinguishable from the major axis pV-diagrams of other, often more highly tilted galaxies, they illustrate an interesting point. In those galaxies, the existence of a compact central feature with a steep linear velocity gradient is often interpreted as the signature of a circular-symmetric physical structure such as e.g. a rotating circumnuclear disk or torus. However, the almost face-on image of M 51 clearly shows the absence of such large-scale structure and the diagrams in Fig. 2 simply reflect the strong molecular enhancement of the inner spiral arms.

Table 4. Integrated line ratios in the centre of M 51.

Transitions	Center		NW Arm GMA-1	
	Observed	Modelled[a]	Observed	Modelled[a]
^{12}CO (1–0)/(2–1)[b]	1.25 ± 0.10	1.28	1.40 ± 0.20	1.35
^{12}CO (3–2)/(2–1)[c]	0.78 ± 0.23	0.75	1.02 ± 0.16	0.87
^{12}CO (4–3)/(2–1)[c]	0.49 ± 0.10	0.41	0.44 ± 0.08	0.46
^{12}CO/ ^{13}CO (1–0)[d]	7 ± 1.5	6.7	8 ± 1.5	8.2
^{12}CO/ ^{13}CO (2–1)[c,d]	6 ± 1	6.9	8.7 ± 1.2	8.1
^{12}CO/ ^{13}CO (3–2)[e]	12.9 ± 1.8	12.2	12.5 ± 1.7	13.2
CI/CO(2–1)[c]	0.22 ± 0.06	–	0.24 ± 0.08	–
CII/CO(2–1)[f]	0.46 ± 0.09	–	–	–

Notes: [a] See Table 5. [b] Ratios estimated from data by Nakai et al. (1994), NRO at 16″ resolution; García-Burillo et al. (1993b), IRAM at 22″. [c] This Paper, JCMT at 21″ resolution. [d] Ratios estimated from data presented by Rickard & Blitz (1985), NRAO 65″, García-Burillo et al. (1993b), IRAM at 22″, Matsushita et al. (1997), NMA at 6″; and Paglione et al. (2001), FRAO at 45″ resolution. [e] This Paper; JCMT at 14″ resolution. f. From Crawford et al. (1985) and Stacey et al. (1991), KAO at 55″ resolution; consistent with ISO flux (Negishi et al. 2001); JCMT convolved to 55″ resolution.

3.2. Line ratios

Using our own and literature data, we have determined line intensity ratios of the observed transitions at both the center (position A), and at the position of the molecular cloud complex in the northwestern arm (position B). All ^{12}CO line ratios listed in Table 4 are for a 21″ beam (roughly corresponding to a circle of 0.5 kpc radius). The isotopic intensity ratios ^{12}CO/ ^{13}CO also refer to that beam size in the $J = 1-0$ and $J = 2-1$ transitions, but to a smaller 14″ beam in the $J = 3-2$ transition. However, the isotopic intensity ratios appear to vary little in the inner part of M 51 (cf. lit. cited) so that we expect that observation with a larger beam would have yielded very similar values for the $J = 3-2$ transition. Note that the [CII]/CO(2–1) ratio was determined after convolution of the $J = 2-1$ ^{12}CO map to the 55″ beam of the [CII] observations. The [CII] intensities (Crawford et al. 1985; Stacey et al. 1991; see also Negishi et al. 2001) were converted to velocity-integrated temperatures to obtain the line ratios in Table 4.

The ^{12}CO and ^{13}CO ratios of M 51 are quite different from those of the other galaxies (NGC 6946, M 83, IC 342, Maffei 2; Israel & Baas 2001, 2003) we have studied so far. The ratio of [CI] to $J = 2-1$ ^{12}CO intensities is relatively high, but that of [CII] to $J = 2-1$ ^{12}CO is not dissimilar from those seen in other galaxies. It resembles, in particular, the ratios seen in galaxies with central starbursts. We suspect that this similarity is caused by the large (radius $R \approx 1.3$ kpc) aperture used to measure the [CII] line in M 51. We suspect that the very center of M 51, weak in CO and HI, contributes relatively little, and that most of the emission in the aperture comes from the inner spiral arms with their strong emission from star-forming regions. Bright [CII] emission indicates the occurrence of both high temperatures and high gas densities as the critical values for this transition are $T_{\rm kin} \geq 91$ K and $n \geq 3500\,{\rm cm}^{-3}$. However, such values must be reconciled with the relatively high CO opacities implied by the modest isotopic intensity ratios in the lower CO transitions. In the arm position B, isotopic ratios increase with increasing J level, but at the center position A the isotopic ratio is lowest in the $J = 2-1$ transition. This reflects significant differences in the molecular gas properties at the two positions sampled.

4. Analysis

4.1. Modelling of CO

We have modelled the observed ^{12}CO and ^{13}CO line intensities and ratios with the large-velocity gradient (LVG) radiative transfer models described by Jansen (1995) and Jansen et al. (1994). These provide model line intensities as a function of three input parameters per molecular gas component: gas kinetic temperature $T_{\rm k}$, molecular hydrogen density $n({\rm H_2})$ and the CO column density per unit velocity $N({\rm CO})/{\rm d}V$. By comparing model to observed line *ratios*, we may identify the physical parameters best describing the actual conditions at the observed positions. Beam-averaged properties are determined by comparing observed and model intensities. In principle, with seven measured line intensities of two isotopes, properties of a single gas component are overdetermined as only five independent observables are required. We found that no fit based on a single gas component is capable of matching the data at either of the observed positions. A similar conclusion was reached by Kramer et al. (2005).

However, we obtained good fits based on *two* gas components. In order to reduce the number of free parameters, we assumed identical CO isotopical abundances for both gas components. In a small number of starburst galaxy centers (NGC 253, NGC 4945, M 82, IC 342, He 2-10), values of 40 ± 10 have been suggested for the isotopical abundance [^{12}CO]/[^{13}CO] (Mauersberger & Henkel 1993; Henkel et al. 1993, 1994, 1998; Bayet et al. 2004), somewhat higher than the characteristic value of 20–25 for the Milky Way nuclear region (Wilson & Rood 1994). Although M 51 does not have a starburst nucleus but rather a low-luminosity AGN, vigorously starforming spiral arms already occur at small radii. For this reason we have adopted an abundance value of [^{12}CO]/[^{13}CO] = 40 in our models. We identified acceptable fits by searching a grid of model parameter combinations (10 K $\leq T_{\rm k} \leq$ 150 K,

Table 5. Model parameters.

Model	Component 1			Component 2			Relative
	Kinetic temperature T_k (K)	Gas density $n(H_2)$ (cm^{-3})	CO column density $N(CO)/dV$ ($cm^{-2}(km\ s^{-1})^{-1}$)	Kinetic temperature T_k (K)	Gas density $n(H_2)$ (cm^{-3})	CO column density $N(CO)/dV$ ($cm^{-2}(km\ s^{-1})^{-1}$)	$J = 2-1$ ^{12}CO emission component 1:2
1 (Center)	100	100	1.0×10^{17}	60	1000	3.0×10^{17}	0.65:0.35
2 (Center)	150	1000	0.6×10^{17}	20	3000	3.0×10^{17}	0.55:0.45
3 (Arm)	100	100	1.0×10^{17}	150	1000	3.0×10^{17}	0.80:0.20

Table 6. Beam-averaged results.

Model	Beam-averaged column densities			Face-on mass density		Relative mass components 1:2	Ratio $N(H_2)/I(CO)$
	$N(CO)$	$N(C)$	$N(H_2)$	$\sigma(H_2)$	σ^a_{gas}		X
	(10^{18} cm^{-2})		(10^{21} cm^{-2})	($M_\odot/pc^{-2}$)			(10^{20} mol cm^{-2}/ K km s^{-1})
M 51; $N_H/N^b_C = 1250$; $N(HI)^c = 2 \times 10^{20}$ cm^{-2}							
1	0.36	4.4	2.9	43	60	0.6 : 0.4	0.74
2	0.36	1.2	1.0	15	20	0.4 : 0.6	0.25
3	0.42	3.3	2.2	33	47	0.8 : 0.2	0.41

Note: [a] Sum of H_2 and HI multiplied by 1.35 to take into account the contribution by helium; [b] See text, Sect. 4.2; [c] HI column density valid for both Center and (nearby) Arm; Tilanus & Allen (1991).

$10^2\,cm^{-3} \le n(H_2) \le 10^5\,cm^{-3}$, $6 \times 10^{15}\,cm^{-2} \le N(CO)/dV \le 3 \times 10^{18}\,cm^{-2}$) for model line ratios matching the observed set, with the relative contribution of the two components as a free parameter. Solutions obtained in this way are not unique, but rather delineate a range of values in distinct regions of parameter space. For instance, variations in input parameters may to some extent compensate one another, producing identical line ratios for somewhat different combinations of input parameters. Among all possible solution sets, we have in any case rejected those in which the denser gas component is also hotter than the more tenuous component, because we consider the large pressure imbalances implied by such solutions physically implausible, certainly on the kiloparsec scales observed.

The results for the two positions in M 51 are summarized in Table 5. The physical conditions applying to the molecular complex in the arm (position B) are very well determined by the observations. The emission is wholly dominated by fairly hot gas with a kinetic temperature of the order of $T_{kin} = 100$ K. Low-density gas with $n_{H_2} \approx 100\,cm^{-3}$ contributes most ($80 \pm 10\%$) of the observed emission, the remainder ($20 \pm 10\%$) coming from gas at a moderately high density $n_{H_2} \approx 1000\,cm^{-3}$ (fortuitously, the masses of the two components are in almost the same proportion – cf. Table 6). These parameters provide a very good fit as is evident from Table 4; no other set of values does.

In contrast, the physical conditions determining the emission from the center of M 51 are more difficult to pin down. Within the errors, two large sets of conditions yield line ratios consistent with the observed values. The first set is very similar to the arm conditions found above: about two thirds of the emission must come from relatively hot, fairly tenuous gas ($T_{kin} \approx 100$ K; $n_{H_2} \approx 100\,cm^{-3}$) while the remainder is contributed by denser and cooler gas ($T_{kin} = 40 \pm 20$ K; $n_{H_2} \approx 1000\,cm^{-3}$). The second set of possible solutions requires all emission to come from moderately dense ($n_{H_2} = 1000-3000\,cm^{-3}$) gas. Half of the emission is then contributed by fairly cold ($T_{kin} \approx 20$ K) and half by fairly warm ($T_{kin} \approx 150$ K) gas. The present observations do not allow us to distinguish between these two possibilities; both are equally likely.

4.2. Beam-averaged molecular gas properties

The chemical models presented by van Dishoeck & Black (1988) show a strong dependence of the $N(C)/N(CO)$ column density ratio (i.e. how much more carbon there is than the fraction tied up in carbon monoxide) on the total carbon and molecular hydrogen column densities. It thus provides a relation between the amounts of carbon monoxide, neutral carbon and ionized carbon that produce the observed line intensities from CO, C°, and C^+. In our analysis, we have assumed that the kinetic temperatures, H_2 densities and filling factors implied by the CO analysis equally apply to the [CI] and [CII] emission. In principle, one can then solve for column densities $N(CI)/dV$ and $N(CII)/dV$. In practice, the column density of one component is usually well-determined, but that of the other is more or less degenerate. For this reason, we solved for identical velocity dispersions in the two gas components. Finally, we related total carbon (i.e. $C^\circ + C^+ + CO$) column densities to molecular hydrogen column densities by using an estimated [C]/[H] gas-phase abundance ratio.

Although the analysis in terms of two gas components is rather superior to that assuming a single component, it is still not fully realistic. For instance, the assumption of identical beam-filling factors or identical velocity dispersions for

the various species (^{12}CO, ^{13}CO, C°, and C$^+$) is not a priori plausible. Fortunately, these assumptions are useful but not critical in the determination of beam-averaged parameters. If, by way of example, we assume a smaller beam-filling factor, the model cloud intensity increases. This generally implies a higher model column-density which, however, is more strongly diluted by the beam. The beam-averaged column-density is modified only by the degree of nonlinearity in the response of the model parameters to a change in filling factor, *not* by the magnitude of that change.

Oxygen abundances and gradients for M 51 were taken from Vila-Costas & Edmunds (1992) and Zaritzky et al. (1994). From the results published by Garnett et al. (1999) we estimate that at the relevant high metallicities [C]/[O] ≈ 1, leading us to adopt a carbon abundance [C]/[H] = [O]/[H] = $3.0 \pm 0.5 \times 10^{-3}$. As a significant fraction of carbon is tied up in dust particles and thus unavailable in the gas-phase, we have adopted a fractional correction factor $\delta_c = 0.27$ (see for instance van Dishoeck & Black 1988), so that $N_H/N_C = [2N(H_2) + N(HI)]/[N(CO) + N(CII) + N(CI)] = 1250$, uncertain by about a factor of two. In Table 6 we present beam-averaged column densities for both CO and C (C° + C$^+$), and H_2 column densities derived under the assumptions just discussed, as well as the face-on mass densities. As the observed peak CO intensities are significantly below the model peak intensities, only a small fraction of the (large) beam surface area can be filled with emitting material. For position A (central region) we find a beam area filling factor of 70 ± 15 for either model, whereas we find a filling factor of about 20 for position B (the spiral arm CO complex).

In order to gauge the reliability of these results, we have explored the effect of the assumptions discussed above. If we do not assume identical velocity dispersions for the two gas components, but e.g. dispersions proportional to the kinetic temperature, derived H_2 columns and mass-densities change by amounts varying from 10% to 20% in the three models described. If we do not assume equal beam filling factors for CO and C$^+$ (which greatly exceeds the contribution by C°, see below), but vary that of C$^+$ by e.g a factor of two, resulting H_2 columns and mass-densities change by amounts varying from 25% to 30%. Differences in beam-filling factors cannot be very much larger, because then the CO and [CII] intensities, the [C]/[H] and [C]/[CO] abundances, and the H_2 column densities become mutually incompatible.

4.3. Discussion

As mentioned above, conditions in the center are fully described by either of two models that cannot be distinguished as both are fully consistent with the observed line ratios and intensities. Observations with much higher resolution using the Smithsonian Millimeter Array (SMA) recovered only a small fraction of the total $J = 3{-}2$ ^{12}CO flux. They showed, however, the existence of a compact (a few arcsec in size) molecular cloud centered on the nucleus (Matsushita et al. 2004) not resolved in our maps. For this cloud, the authors estimated high densities and temperatures that seem more or less consistent with those of our Model 2/Component 1. However, as they used only single-component LVG fitting such resemblance may be fortuitous.

Our two models have in common that they explain the observed emission by requiring the existence of at least two gas components at different densities and temperatures. Nevertheless, they imply very different ISM conditions as these kinetic temperatures and densities vary significantly between models. The implied hydrogen column densities, mass surface densities and CO-to-H_2 conversion factor X also differ significantly, by a factor of three. That difference is almost entirely caused by the fact that at lower kinetic temperatures a much larger ionized carbon (C$^+$) column density is required to produce the *same observed [CII] line flux* than at higher kinetic temperatures.

Beam-averaged *neutral* carbon to carbon monoxide column density ratios range from $N(C^o)/N(CO) = 0.4$–1.0, and are very comparable to those found in other galaxy centers (White et al. 1994; Israel et al. 1995; Stutzki et al. 1997; Petitpas & Wilson 1998; Israel & Baas 2001, 2003).

Our model results agree well with the parameters that we would have obtained by applying the PDR models presented by Kaufman et al. (1999) to the observed intensities and ratios of the CO, [CI], [CII] lines, and the intensity of the far-infrared continuum (Rand et al. 1992). For the observed values, the PDR models predict the presence of molecular gas at temperatures $T_{kin} \approx 100$ K, and at gas densities 10^3 cm^{-3} illuminated by a fairly modest ambient radiation field with log $G_o = 1.0$ (G_o expressed in units of the Habing 1968 field: 1.6×10^{-3} erg s^{-1} cm^{-2}).

Our models also imply the central regions of M 51 to have a CO-to-H_2 conversion factor $X = 0.50 \pm 0.25 \times 10^{20}$ H_2 mol cm^{-2}/ K km s^{-1}, i.e. roughly a factor of four lower than the commonly used Galactic X value for the Solar Neighbourhood. However, such low values are not uncommon for galactic centers (Israel & Baas 2003 and references therein). For M 51, virtually identical results have also been obtained independently by Guélin et al. (1995) from an analysis of the 1.2 μm emission from cold dust, and by Nakai & Kuno (1995) when one considers their results for HII regions with one arcminute from the nucleus. Thus, we consider that the CO-to-H_2 conversion factor X is unusually well-established in the center of M 51; there can be little doubt that it is indeed much lower than the "standard" Milky Way value (see also Strong et al. 2004). We emphasize that low values for X mean that for any given CO intensity, beam-averaged molecular hydrogen column densities $N(H_2)$ and indeed H_2 masses are much less than estimated from the "standard" conversion. This has another important implication. All *molecular species abundances* derived by relating an independently determined column density to a molecular hydrogen column density obtained from the "standard" Galactic conversion factor are in error and *must be revised upwards* by a potentially large factor.

5. Conclusions

1. Observation of the central arcminute of the well-studied spiral galaxy M 51 in various transitions of ^{12}CO

and ^{13}CO, and in [CI] shows that the molecular gas resides mostly in the bright inner spiral arms.

2. The absence of a circumnuclear disk or torus in images of the center of M 51 whereas position-velocity maps exhibit a compact central feature exhibiting a rapid solid-body rotation implies that in other galaxies the presence of the latter cannot be taken as proof for the presence of the former.
3. In the center of M 51, a dense component with $n(\mathrm{H_2}) \approx 10^3\,\mathrm{cm^{-3}}$ and $T_{\rm kin} \approx 100$ K is accompanied by either a *less dense* component with $n(\mathrm{H_2}) \approx 10^2\,\mathrm{cm^{-3}}$ at the same temperature, or a *more dense* component with $n(\mathrm{H_2}) \approx 3 \times 10^3\,\mathrm{cm^{-3}}$ at a much lower temperature of $T_{\rm kin} \approx 20$ K. Only a small fraction of all carbon is in CO. Total carbon column densities are about 7 times the CO column density. At least in the center of M 51, most of the carbon appears to be in the form of C^+. The observed line ratios are consistent with standard PDR models.
4. Emission from the CO peak in the northwestern arm likewise originates in (at least) two different gas components. One is modestly dense ($n(\mathrm{H_2}) \approx 10^3\,\mathrm{cm^{-3}}$) and the other is relatively tenuous ($n(\mathrm{H_2}) \approx 10^2\,\mathrm{cm^{-3}}$) but more widespread. Both must be at elevated temperatures $T_{\rm kin} = 100{-}150$ K.
5. The center of M 51 has a face-on gas mass density of $40 \pm 20\ M_\odot\ \mathrm{pc^{-2}}$, and a relatively well-established CO-to-H_2 conversion factor $X = 0.50 \pm 0.25 \times 10^{20}\,\mathrm{H_2\ mol\ cm^{-2}/\,K\,km\,s^{-1}}$, i.e. a factor of four to five lower than commonly assumed standard Galactic values, but in line with similar determinations in other galaxy centers.

Acknowledgements. We are indebted to Ewine van Dishoeck and David Jansen for providing us with their detailed radiative transfer models. We thank the JCMT personnel for their support and help in obtaining the observations discussed in this paper.

References

Aalto, S., Hüttemeister, S., Scoville, N. Z., & Thaddeus, P. 1999, ApJ, 522, 165

Bayet, E., Gerin, M., Phillips, T. G., & Contursi, A. 2004, A&A, 427, 45

Berkhuijsen, E. M., Bajaja, E., & Beck, R. 1993, A&A, 279, 357

Crawford, M. K., Genzel, R., Townes, C. H., & Watson, D. M. 1985, A&A, 291, 755

Dumke, M., Nieten, Ch., Thuma, G., Wielebinski, R., & Walsh, W. 2001, A&A, 373, 853

García-Burillo, S., Combes, F., & Gerin, M. 1993a, A&A, 274, 148

García-Burillo, S., Guélin, M., & Cernicharo, J. 1993b, A&A, 274, 123

Garnett, D. R., Shields, G. A., Peimbert, M., et al. 1999, ApJ, 513, 168

Guélin, M., Zylka, R., Mezger, P. G., Haslam, C. G. T., & Kreysa, E. 1995, A&A, 298, 29

Habing, H. J. 1969, Bull. Astron. Inst. Netherlands, 19, 421

Henkel, C., Mauersberger, R., Wiklind, T., et al. 1993, A&A, 268, L17

Henkel, C., Whiteoak, J. B., & Mauersberger, R. 1994, A&A, 284, 17

Henkel, C., Chin, Y.-N, Mauersberger, R., & Whiteoak, J. B. 1998, A&A, 329, 443

Israel, F. P., & Baas, F. 1999, A&A, 351, 10

Israel, F. P., & Baas, F. 2001, A&A, 371, 433

Israel, F. P., & Baas, F. 2003, A&A, 404, 495

Israel, F. P., White, G. J., & Baas, F. 1995, A&A, 302, 343

Jansen, D. J. 1995, Ph.D. Thesis, University of Leiden (NL)

Jansen, D. J., van Dishoeck, E. F., & Black, J. H. 1994, A&A, 282, 605

Kaufman, M. J., Wolfire, M. G., Hollenbach, D. J., & Luhman, M. L. 1999, ApJ, 527, 795

Kramer, C., Mookerjea, B., Bayet, E., et al. 2005, A&A, 441, 961

Lo, K. Y., Ball, R., Masson, C. R., et al. 1987, ApJ, 317, 63

Matsushita, S., Kohno, K., Vila-Vilaro, B., Tosaki, T., & Kawabe, R. 1998, ApJ, 495, 267

Matsushita, S., Sakamoto, K., Kuo, C.-Y., et al. 2004, ApJ, 616, 55

Mauersberger, R., & Henkel, C. 1993, Rev. Mod. Astron., 6, 69

Mauersberger, R., Henkel, C., Walsh, W., & Schulz, A. 1999, A&A, 341, 256

Nakai, N., Kuno, N., Handa, T., & Sofue, Y. 1994, PASJ, 46, 527

Nakai, N., & Kuno, N. 1995, PASJ, 47, 761

Negishi, T., Onaka, T., Chan, K.-W., & Roellig, T. 2001, A&A, 375, 566

Paglione, T. A. D., Wall, W. F., Young, J. S., et al. 2001, ApJ, 135, 183

Petitpas, G. R., & Wilson, C. D. 1998, ApJ, 503, 219

Rand, R. J. 1993, ApJ, 404, 593

Rand, R. J., & Kulkarni, S. R. 1990, ApJ, 349, 43

Rand, R. J., Kulkarni, S. R., & Rice, W. 1992, ApJ, 390, 66

Regan, M. W., Thornley, M. D., Helfer, T. T., et al. 2001, ApJ, 561, 218

Rickard, L. J., & Blitz, L. 1985, ApJ, 292, L57

Rickard, L. J., Turner, B. E., Palmer, P., Morris, M., & Zuckerman, B. 1977, ApJ, 218, L51

Rydbeck, G., Hjalmarson, Å., & Rydbeck, O. E. H. 1985, A&A, 144, 282

Sakamoto, K., Okumura, S. K., Ishizuki, S., & Scoville, N. Z. 1999, ApJS, 124, 403

Sandage, A., & Tammann, G. A. 1975, ApJ, 196, 313

Sandage, A., & Tammann, G. A. 1987, A Revised Shapley-Ames Catalog of Bright Galaxies, second edition, Carnegie Institution of Washington Publication 635 (Washington, DC: Carnegie Institution of Washington).

Sandqvist, Aa., Elfhag, T., & Lindblad, P. O. 1989, A&A, 218, 39

Scoville, N. Z., &, Young, J. S. 1983, ApJ, 265, 148

Scoville, N. Z., Yun, M. S., Armus, L., & Ford, H. 1998, ApJ, 493, 63

Stacey, G. J., Geis, N., Genzel, R., et al. 1985, A&A, 373, 423

Strong, A. W., Moskalenko, I. V., Reimer, O., Digel, S., & Diehl, R. 2004, A&A, 422, 47

Stutzki, J., Graf, U. U., Honingh, C. E., et al. 1997, ApJ, 477, 33

Tilanus, R. P. J., & Allen, R. J. 1991, A&A, 244, 8

Tosaki, T., Kawabe, R., & Taniguchi, Y. 1994, in Astronomy with Millimeter and Submillimeter Wave Interferometry, IAU Coll. 140, ed. M. Ishiguro, & J. Welch, ASP Conf. Ser., 59, 353

Tosaki, T., Hasegawa, T., Shioya, Y., Kuno, N., & Matsushita, S. 2002, PASJ, 54, 209

Tully, R. B. 1974, ApJS, 27, 437

Turner, J. L., & Ho, P. T. P. 1994, ApJ, 421, 122

van Dishoeck, E. F., & Black, J. H. 1988, ApJ, 334, 771

Vila-Costas, M. B., & Edmunds, M. G. 1992, MNRAS, 259, 121

White, G. J., Ellison, B., Claude, S., Dent, W. R. F., & Matheson, D. 1994, A&A, 284, L23

Wielebinski, R., Dumke, M., & Nieten, Ch. 1999, A&A, 347, 643

Wilson, T. L., & Rood, R. T. 1994, ARA&A, 32, 191

Young, J. S., Xie, S., Tacconi, L., et al. 1995, ApJS, 98, 219

Zaritsky, D., Kennicutt, R. C., & Huchra, J. P. 1994, ApJ, 420, 87